Overfrustrated and underfrustrated spin glasses in $d = 3$ and 2: Evolution of phase diagrams and chaos including spin-glass order in $d = 2$

Efe Ilker[1] and A. Nihat Berker[1,2]

[1]*Faculty of Engineering and Natural Sciences, Sabancı University, Tuzla 34956, Istanbul, Turkey*

[2]*Department of Physics, Massachusetts Institute of Technology, Cambridge, Massachusetts 02139, USA*

(Received 27 November 2013; published 21 April 2014)

In spin-glass systems, frustration can be adjusted continuously and considerably, without changing the antiferromagnetic bond probability p, by using locally correlated quenched randomness, as we demonstrate here on hypercubic lattices and hierarchical lattices. Such overfrustrated and underfrustrated Ising systems on hierarchical lattices in $d = 3$ and 2 are studied. With the removal of just 51% of frustration, a spin-glass phase occurs in $d = 2$. With the addition of just 33% frustration, the spin-glass phase disappears in $d = 3$. Sequences of 18 different phase diagrams for different levels of frustration are calculated in both dimensions. In general, frustration lowers the spin-glass ordering temperature. At low temperatures, increased frustration favors the spin-glass phase (before it disappears) over the ferromagnetic phase and symmetrically the antiferromagnetic phase. When any amount, including infinitesimal, frustration is introduced, the chaotic rescaling of local interactions occurs in the spin-glass phase. Chaos increases with increasing frustration, as can be seen from the increased positive value of the calculated Lyapunov exponent λ, starting from $\lambda = 0$ when frustration is absent. The calculated runaway exponent y_R of the renormalization-group flows decreases with increasing frustration to $y_R = 0$ when the spin-glass phase disappears. From our calculations of entropy and specific-heat curves in $d = 3$, it is shown that frustration lowers in temperature the onset of both long- and short-range order in spin-glass phases, but is more effective on the former. From calculations of the entropy as a function of antiferromagnetic bond concentration p, it is shown that the ground-state and low-temperature entropy already mostly sets in within the ferromagnetic and antiferromagnetic phases, before the spin-glass phase is reached.

DOI: 10.1103/PhysRevE.89.042139 PACS number(s): 64.60.De, 75.10.Nr, 05.10.Cc, 75.50.Lk

I. INTRODUCTION

The occurrence of spin-glass long-range order [1], ground-state entropy [2,3], and chaotic rescaling behavior [4,5] has long been discussed in spin-glass systems, with reference to spatial dimensionality d, interaction randomness, and frustration [6], accepted as inherent to spin-glass systems and spin-glass order. In Ising models with randomly distributed nearest-neighbor ferromagnetic and antiferromagnetic interactions on hypercubic lattices, it has been shown that a spin-glass phase does not occur in $d = 2$ and does occur in $d = 3$ [7]. In these hypercubic systems, frustration occurs in elementary squares with an odd number of antiferromagnetic interactions. Thus, with interactions randomly distributed with no correlation, maximally 50% of the elementary squares can be frustrated. This fraction increases from zero as the concentration of frozen antiferromagnetic bonds p is increased from zero and reaches its maximal value of 50% at $p = 0.5$.

The basis of the current study is the realization that, for any value of the antiferromagnetic bond concentration $0 < p < 1$, the fraction of frustrated squares can be varied considerably. For example, for the square lattice, for $0.25 \leqslant p \leqslant 0.75$, the fraction of frustrated squares can be made to vary to any value between 0 and 1 inclusive, by the locally correlated occurrence quenched random bonds. For $p \leqslant 0.25$, the fraction of frustrated squares can similarly be made to vary between 0 and $4p$. For $0.75 \leqslant p$, the fraction of frustrated squares can be made to vary between 0 and $4(1 - p)$. (Thus, frustration reaches 0 with no variation as p approaches 0 or 1.) Examples are shown in Fig. 1 for $p = 0.5$. Thus, when the fraction of frustrated squares is zero, we have a so-called Mattis spin glass [8]. At the other extreme, we have a fully frustrated system [9–13]. All frustration values in between can be obtained by randomly removing or adding local frustration without changing the antiferromagnetic bond concentration p (Fig. 1).

In this study, we implement an exact renormalization-group study for Ising spin-glass models on the hierarchical lattices, with $d = 3$ and 2, respectively shown in Figs. 2(b) and 3(b), for arbitrary overfrustration or underfrustration implemented

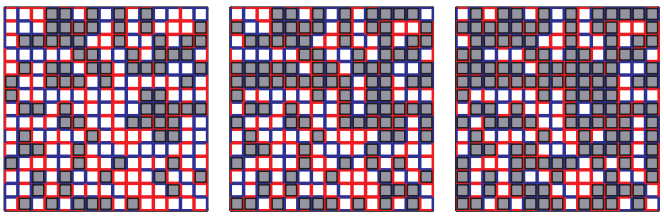

FIG. 1. (Color online) Randomly distributed ferromagnetic (blue) and antiferromagnetic (red) interactions on a square plane. In all three cases, the antiferromagnetic bond concentration is $p = 0.5$. The frustrated squares are shaded. In the case at the center, the bonds were distributed in an uncorrelated fashion, leading to the frustration of half of the squares (stochastic frustration). In the case at the left, 25% of the frustration was randomly removed without changing $p = 0.5$ (underfrustration). In the case at the right, 25% frustration was randomly added without changing $p = 0.5$ (overfrustration). Frustration can thus be set between zero and complete frustration. It is clear that frustration can thus be adjusted in all hypercubic lattices.

by locally correlated quenched randomness. We calculate 18 complete phase diagrams, each for a different frustration level, in temperature and antiferromagnetic bond probability p. We find that the increase of frustration disfavors the spin-glass phase (while at low temperatures favoring the spin-glass phase at the expense of the ferromagnetic phase and, symmetrically, the antiferromagnetic phase.) In both $d = 3$ and 2, the spin-glass phase disappears at zero temperature when a certain level of frustration is reached. However, this disappearance of the spin-glass phase happens in different regimes in $d = 3$ and 2. For $d = 3$, it occurs in overfrustration, so that at stochastic frustration (no correlation in randomness) a spin-glass phase occurs. For $d = 2$, it already occurs in underfrustration, so that at stochastic frustration a spin-glass phase does not occur. However, with frustration only partially removed, we find that a spin-glass phase certainly does occur in $d = 2$.

The chaotic rescaling [4,5,14–35] of the interactions within the spin-glass phase occurs as soon as frustration is increased from zero, in both $d = 3$ and 2. We have calculated the Lyapunov exponent λ [36,37] of the renormalization-group trajectory of the interaction at a given location, when the system is in the spin-glass phase. When frustration is increased from zero, the Lyapunov exponent λ increases from zero, in both $d = 3$ and 2. This behavior is of course consistent with the chaotic renormalization-group trajectories. Different values of the positive Lyapunov exponents characterize different spin-glass phases. It is found here that the value of the Lyapunov exponent continuously varies with the level of frustration and is different for each dimensionality d. The Lyapunov exponent does not depend on antiferromagnetic bond concentration p or temperature.

Our calculations with varying frustration also yield information on long- and short-range ordering and entropy. The increase in frustration lowers both the onset temperature of long-range order and the characteristic temperature of short-range order, but affects long-range order much more drastically, thus interchanging the two temperatures and eventually eliminating long-range spin-glass order. For $d = 3$, for low frustration, the specific-heat peak occurs inside the spin-glass phase, indicating that considerable short-range disorder persists into the higher temperatures of the spin-glass phase. In these cases, as temperature is lowered, spin-glass long-range order onsets before the system is predominantly short-range ordered. As frustration is increased, both ordering temperatures are lowered, but differently, so that they interchange before stochastic frustration is reached. Thus, for overfrustration, stochastic frustration, and higher frustration values of underfrustration, the specific-heat peak occurs outside the spin-glass phase, indicating that as temperature is lowered, short-range order sets before long-range order (which reaches zero temperature in overfrustration). Zero-temperature or low-temperature entropy is a distinctive characteristic of systems with frustration. Frustration is introduced into the system by increasing from zero the antiferromagnetic bond concentration p. It is seen that frustration favors the spin-glass phase over the ferromagnetic phase. However, it is also seen that, in all cases that frustration is introduced, the major portion of the entropy is created within the ferromagnetic phase as opposed to the spin-glass phase.

II. OVERFRUSTRATED AND UNDERFRUSTRATED SPIN-GLASS SYSTEMS ON HYPERCUBIC LATTICES AND HIERARCHICAL LATTICES

A. Stochastic frustration, overfrustration, and underfrustration on hypercubic lattices

The Ising spin-glass model is defined by the Hamiltonian

$$-\beta\mathcal{H} = \sum_{\langle ij\rangle} J_{ij} s_i s_j, \tag{1}$$

where $\beta = 1/kT$, at each site i of a lattice the spin $s_i = \pm 1$, and $\langle ij\rangle$ denotes that the sum runs over all nearest-neighbor pairs of sites. The bond strengths J_{ij} are $J > 0$ (ferromagnetic) with probability $1 - p$ and $-J$ (antiferromagnetic) with probability p. On hypercubic lattices, in any elementary square with an odd number number of antiferromagnetic bonds, all bonds cannot be simultaneously satisfied, meaning that there is frustration [6]. When the antiferromagnetic bonds are randomly distributed with probability p across the lattice, a fraction

$$4p(1-p)^3 + 4p^3(1-p) = 4(p - 3p^2 + 4p^3 - 2p^4) \tag{2}$$

of the elementary squares is frustrated. This system with uncorrelated quenched randomness is the usually studied spin-glass system and we shall refer to it as a **stochastically frustrated** system. On the other hand, by changing the signs of individual bonds $J_{ij} \to -J_{ij}$ at randomly chosen localities, with the rule that, for every ferromagnetic-to-antiferromagnetic local change, an antiferromagnetic-to-ferromagnetic local change is done, frustration can be continuously increased or decreased from the value in Eq. (2), without changing the antiferromagnetic bond concentration p. We call the systems in which frustration is thus increased or decreased from stochastic frustration, respectively, **overfrustrated** or **underfrustrated** systems. Examples of overfrustration, stochastic frustration, and underfrustration are given in Fig. 1.

B. Renormalization-group transformation, quenched probability convolutions by histograms and cohorts

The usual, stochastically frustrated spin-glass systems on hypercubic lattices are readily solved by a renormalization-group method that is approximate on the hypercubic lattice [38,39] and simultaneously exact on the hierarchical lattice [40–44]. Under rescaling, the form of the interaction as given in Eq. (1) is conserved. The renormalization-group transformation, for spatial dimension d and length-rescaling factor $b = 3$ (necessary for treating the ferromagnetic and antiferromagnetic correlations on equal footing), is achieved [Figs. 2(a) and 3(a)] by a sequence of bond moving

$$J_{ij}^{(bm)} = \sum_{\langle kl\rangle}^{b^{d-1}} J_{kl} \tag{3}$$

and decimation

$$e^{J_{im}^{(dec)} s_i s_m + G_{im}} = \sum_{s_j, s_k} e^{J_{ij} s_i s_j + J_{jk} s_j s_k + J_{km} s_k s_m}, \tag{4}$$

where the additive constants G_{ij} are unavoidably generated.

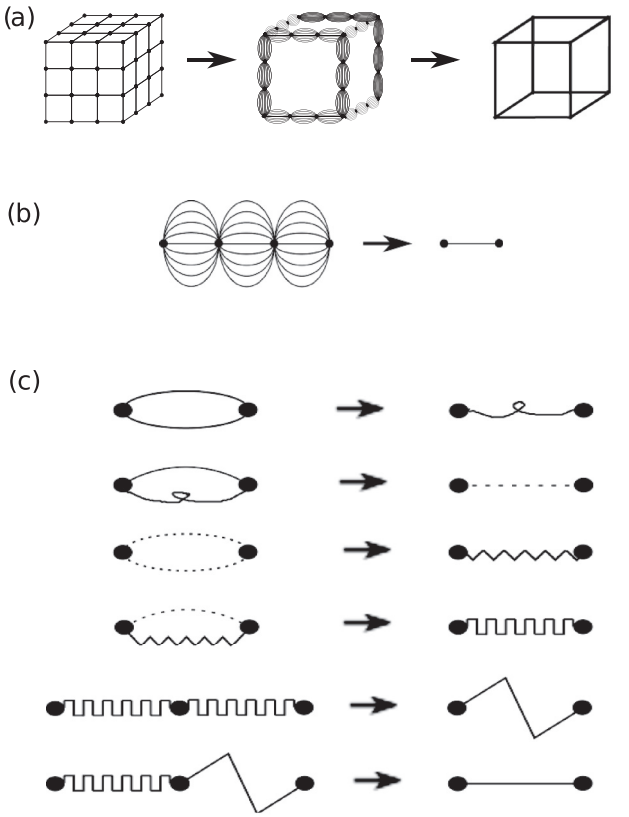

FIG. 2. (a) Migdal-Kadanoff approximate renormalization-group transformation for the $d = 3$ cubic lattice with the length-rescaling factor of $b = 3$. Bond moving is followed by decimation. (b) Exact renormalization-group transformation for the equivalent $d = 3$ hierarchical lattice with the length-rescaling factor of $b = 3$. (c) Pairwise applications of the quenched probability convolution of Eq. (5), leading to the exact transformation in (b) and to the numerically equivalent approximate transformation in (a).

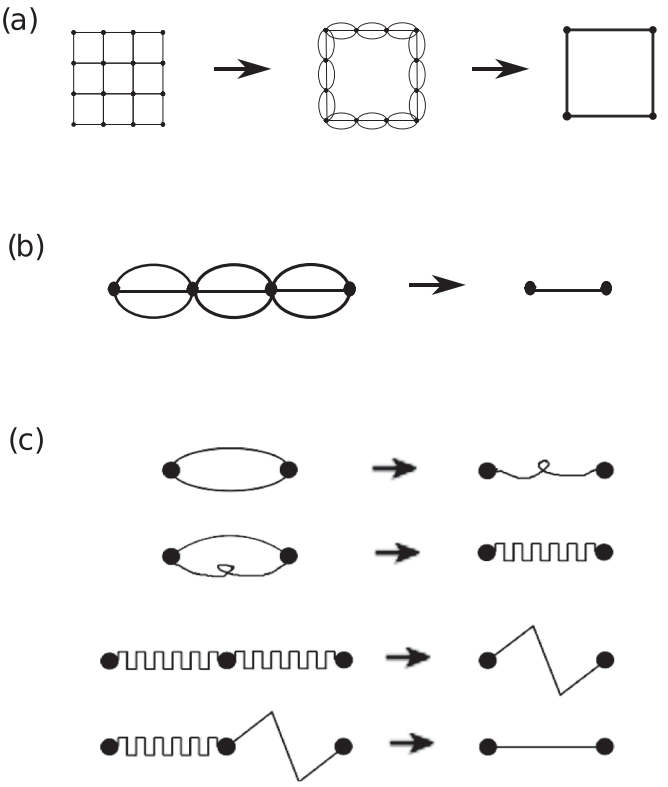

FIG. 3. (a) Migdal-Kadanoff approximate renormalization-group transformation for the $d = 2$ square lattice with the length-rescaling factor of $b = 3$. Bond moving is followed by decimation. (b) Exact renormalization-group transformation for the equivalent $d = 2$ hierarchical lattice with the length-rescaling factor of $b = 3$. (c) Pairwise applications of the quenched probability convolution of Eq. (5), leading to the exact transformation in (b) and to the numerically equivalent approximate transformation in (a).

The starting bimodal quenched probability distribution of the interactions, characterized by p and described above, is not conserved under rescaling. The renormalized quenched probability distribution of the interactions is obtained by the convolution [45]

$$P'(J'_{i'j'}) = \int \left[\prod_{ij}^{i'j'} dJ_{ij} P(J_{ij}) \right] \delta(J'_{i'j'} - R(\{J_{ij}\})), \quad (5)$$

where the primes denote the renormalized system and $R(\{J_{ij}\})$ represents the bond moving and decimation given in Eqs. (3) and (4). For numerical practicality, the bond moving and decimation of Eqs. (3) and (4) are achieved by a sequence of pairwise combination of interactions, as shown for $d = 3$ and 2, respectively, in Figs. 2(c) and 3(c), each pairwise combination leading to an intermediate probability distribution resulting from a pairwise convolution as in Eq. (5).

We implement this procedure numerically in two calculationally equivalent ways: (i) The quenched probability distribution is represented by histograms [46–49]. A total number of between 500 to 2500 histograms, depending on the needed accuracy, is used here. This total number is distributed between ferromagnetic $J > 0$ and antiferromagnetic $J < 0$ interactions according to the total probabilities for each case. (ii) A cohort of 20 000 interactions [31] that embodies the quenched probability distribution is generated. At each pairwise convolution as in Eq. (5), 20 000 randomly chosen pairs are matched by Eq. (3) or (4) and a new set of 20 000 is produced. The numerical convergence of the histogram and cohort implementations are determined, respectively, by the numbers of histograms and cohort members. At numerical convergence, the results of the two implementations match. The histogram method is faster and is used to calculate phase diagrams, thermodynamic properties, and asymptotic fixed distributions. The cohort method is needed for studying the repeated rescaling behavior of the interaction at a specific location on the lattice and is used to calculate chaotic trajectories, chaotic bands, and Lyapunov exponents [31].

C. Stochastic frustration, overfrustration, and underfrustration on hierarchical lattices

Hierarchical models are models which are exactly soluble by renormalization-group theory [40–44]. Hierarchical lattices have therefore been used to study a variety of spin-glass and other statistical mechanics problems [46–58]. Hierarchical models can be constructed [40] that have

identical renormalization-group recursion relations with the approximate treatment of models on hypercubic and other Euclidian lattices. Thus, Figs. 2(b) and 3(b) respectively give the hierarchical models, used in our study, that have the same recursion relations as the Migdal-Kadanoff approximation [38,39] for the hypercubic lattice in $d = 3$ (cubic lattice) and $d = 2$ (square lattice).

Overfrustration or underfrustration is readily introduced into hierarchical lattices by randomly changing local interactions or groups of local interactions while conserving p. This overfrustration or underfrustration affects the pairwise bond-moving step of the renormalization-group solution. In the case of overfrustration, when two bonds are matched for bond moving, bonds of the same sign are accepted with a probability g, $0 \leq g < 1$. Clearly, when $g = 1$, we have not altered the occurrence of frustration; however, for a value of g in the range $0 \leq g < 1$, we have removed a fraction $1 - g$ of the unfrustrated occurrences.

Similarly, in the case of underfrustration, when two bonds are matched for bond moving, bonds of the opposite sign are accepted with a probability $f, 0 \leq f < 1$. Again, when $f = 1$, we have not altered the occurrence of frustration; however, for a value of f in the range $0 \leq f < 1$, we have removed a fraction $1 - f$ of the frustrated occurrences.

We have thus defined the degree of frustration on the hierarchical models. Accordingly, full frustration, stochastic frustration, and zero frustration respectively correspond to $g = 0$, $g = 1 = f$, and $f = 0$. Our implementation of underfrustration and overfrustration via the factors f and g does affect, on the hierarchical lattice, the effective value of the antiferromagnetic bond probability p as

$$p_{\text{effective}} = \frac{p - (1-f)p(1-p)}{1 - (1-f)2p(1-p)},$$
$$p_{\text{effective}} = \frac{p - (1-g)p^2}{1 - (1-g)[p^2 + (1-p)^2]}. \quad (6)$$

Here $p_{\text{effective}}$ includes the combined effect of p together with the local quenched correlation rule controlled by f or g. (The actual microscopic renormalization-group calculation is of course done using p with the quenched correlation rule, which completely defines the model.) Equations (6) directly follow from the acceptance rules given in the previous two paragraphs: The second terms in the numerators subtract the probability due to rejection because of a bond-moving match that is suppressed; the denominator is a normalization taking into account this rejection probability. Thus, $p = 0.5$, the center of a would-be spin-glass phase, is not affected. For other values, $p_{\text{effective}}$ stays close to p, as shown in Fig. 4. Just as in the case of underfrustrated and overfrustrated hypercubic lattices (Fig. 1), underfrustrated and overfrustrated hierarchical lattices as defined and studied here can be physically realized. However, our procedure of underfrustrating or overfrustrating hierarchical lattices is not a direct representation of underfrustrating or overfrustrating hypercubic lattices. One important difference is that, in hierarchical lattices, underfrustrating or overfrustrating is done at every length scale. This leaves the underfrustrated or overfrustrated hypercubic lattices, which can be achieved as we demonstrated, as an interesting open problem, with our current results only being suggestive.

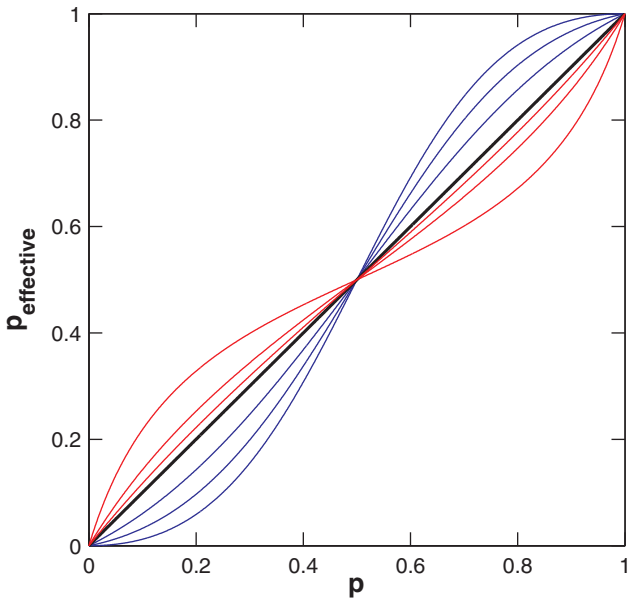

FIG. 4. (Color online) Plot of $p_{\text{effective}}$ versus p for the range of underfrustration and overfrustration used in our study [Eq. (6)]. The curves are, consecutively from the lower right, for $f = 0,0.2,0.5$; $f = 1 = g$ (thicker line); and $g = 0.8,0.6,0.3$.

D. Determination of the phase diagrams and thermodynamic properties

The different thermodynamic phases of the model are identified by the different asymptotic renormalization-group flows of the quenched probability distributions. For all renormalization-group flows, inside the phases and on the phase boundaries, Eq. (5) is iterated until asymptotic behavior is reached, meaning that we are studying an effectively infinite hierarchical lattice. The thermodynamic properties, such as free energy, energy, entropy, and specific heat, are calculated by summing along entire renormalization-group trajectories [40,43,44,59]. Thus, we are able to calculate phase diagrams and thermodynamic properties for any case of overfrustration or underfrustration.

III. CALCULATED PHASE DIAGRAMS FOR OVERFRUSTRATION AND UNDERFRUSTRATION IN $d = 3$ AND 2

Figure 5 shows 18 different calculated phases diagrams, in temperature $1/J$ and antiferromagnetic bond concentration p, for overfrustrated, stochastically frustrated, and underfrustrated Ising spin-glass models in $d = 3$ and 2. Each phase diagram has a different amount of overfrustration or underfrustration, or is stochastically frustrated. In general, increased frustration drives the spin-glass phase to lower temperatures. Thus, the spin-glass phase disappears at a threshold amount of frustration. This threshold frustration is dramatically different in $d = 3$ and 2, as explained below. On the other hand, increased frustration favors the spin-glass phase (before it disappears) over the ferromagnetic phase and symmetrically the antiferromagnetic phase, at low temperatures.

The left panels are for $d = 3$ dimensions. The outermost phase diagram, consisting of one horizontal and two vertical

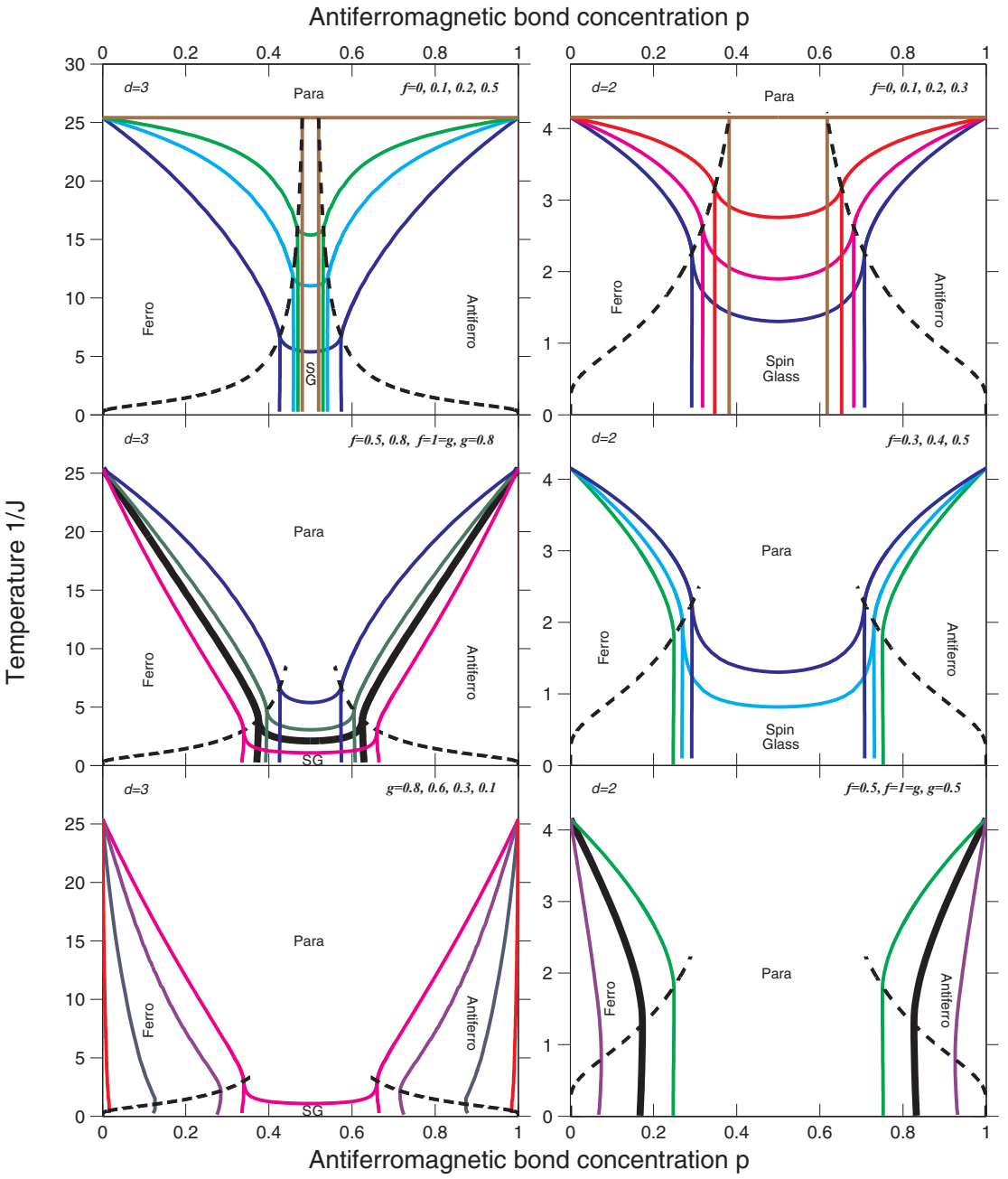

FIG. 5. (Color online) Calculated phase diagrams of the overfrustrated, underfrustrated, and stochastically frustrated Ising spin-glass models on hierarchical lattices. The panels on the left side are for $d = 3$ dimensions. In the left top panel, the outermost phase diagram, consisting of one horizontal and two vertical lines, is for no frustration, $f = 0$. Starting from this outermost phase diagram, the three consecutive phase diagrams are for the underfrustrated cases (where frustration has been removed) of $f = 0.1,0.2,0.5$. In the left middle panel, starting from the outermost phase diagram, the four consecutive phase diagrams are for the underfrustrated cases of $f = 0.5,0.8$; the stochastic case (where frustration has been neither removed nor added) of $f = 1 = g$, drawn with the thicker lines; and the overfrustrated case (where frustration has been added) of $g = 0.8$. In the left bottom panel, starting from the outermost phase diagram, the four consecutive phase diagrams are for the overfrustrated cases of $g = 0.8,0.6,0.3,0.1$. In the latter three cases, $g = 0.6,0.3,0.1$, no spin-glass phase occurs. Excessive overfrustration destroys the spin-glass phase. The panels on the right side are for $d = 2$ dimensions. In the right top panel, the outermost phase diagram, consisting of one horizontal and two vertical lines, is for no frustration, $f = 0$. Starting from this outermost phase diagram, the three consecutive phase diagrams are for the underfrustrated cases of $f = 0.1,0.2,0.3$. In the right middle panel, starting from the outermost phase diagram, the three consecutive phase diagrams are for the underfrustrated cases of $f = 0.3,0.4,0.5$. In the right bottom panel, starting from the outermost phase diagram, the three consecutive phase diagrams are the underfrustrated case of $f = 0.5$; for the stochastic case of $f = 1 = g$, drawn with the thicker lines; and the overfrustrated case of $g = 0.5$. In the latter three cases, $f = 0.5, f = 1 = g, g = 0.5$, no spin-glass phase occurs. However, in the underfrustrated cases of $f = 0.1,0.2,0.3,0.4$, a spin-glass phase occurs in these $d = 2$ dimensional systems with locally correlated randomness. All phase transitions in this figure are second order and, to the resolution of the figure, all multicritical points appear on the Nishimori symmetry line, shown with the dashed curves.

lines, is for no frustration, $f = 0$. Starting from this outermost phase diagram, the consecutive phase diagrams have increasing frustration: They are for the underfrustrated cases (where frustration has been removed) of $f = 0.1,0.2,0.5,0.8$; the stochastic case (where frustration has been neither removed nor added) of $f = 1 = g$, drawn with the thicker lines; and the overfrustrated cases (where frustration has been added) of $g = 0.8,0.6,0.3,0.1$. In the latter three cases, $g = 0.6,0.3,0.1$, no spin-glass phase occurs. Thus, in $d = 3$, excessive overfrustration destroys the spin-glass phase.

The right panels are for $d = 2$ dimensions. Again, the outermost phase diagram, consisting of one horizontal and two vertical lines, is for no frustration, $f = 0$. Starting from this outermost phase diagram, the consecutive phase diagrams again have increasing frustration: They are for the underfrustrated cases of $f = 0.1,0.2,0.3,0.4,0.5$; the stochastic case of $f = 1 = g$, drawn with the thicker lines; and the overfrustrated case of $g = 0.5$. In the latter three cases, $f = 0.5$, $f = 1 = g$, and $g = 0.5$, no spin-glass phase occurs. However, in the underfrustrated cases of $f = 0.1,0.2,0.3,0.4$, a spin-glass phase does occur in these $d = 2$ dimensional systems with locally correlated randomness. Thus, when frustration is increased from zero, the spin-glass phase disappears while still in the underfrustrated regime. Accordingly, in ordinarily studied spin-glass systems, which are stochastically frustrated systems, the spin-glass phase is seen in $d = 3$, but not in $d = 2$.

The paramagnetic–ferromagnetic–spin-glass reentrance for the phase diagrams with the spin-glass phase and the paramagnetic-ferromagnetic-paramagnetic (true) reentrance for the phase diagrams without the spin-glass phase, as temperature is lowered, is seen here. Both types of phase diagrams were first noted with hierarchical models for Ising spin glasses [46] and Potts spin glasses [51]. Phase diagram reentrance is also seen in experimental spin-glass systems [60] and preeminently in liquid-crystal systems where annealed (as opposed to quenched, as in the current study) frustration plays a role [61–64]. All phase transitions in Fig. 5 are second order and, to the resolution of the figure, the multicritical points appear on the Nishimori symmetry line, shown with the dashed curves [65–69].

IV. CHAOS IN THE SPIN-GLASS PHASE TRIGGERED BY INFINITESIMAL FRUSTRATION

The local interaction at a given position in the lattice at successive renormalization-group transformations, in systems with different frustrations, is given for $d = 3$ and 2, respectively, in Figs. 6 and 7. These consecutively renormalized

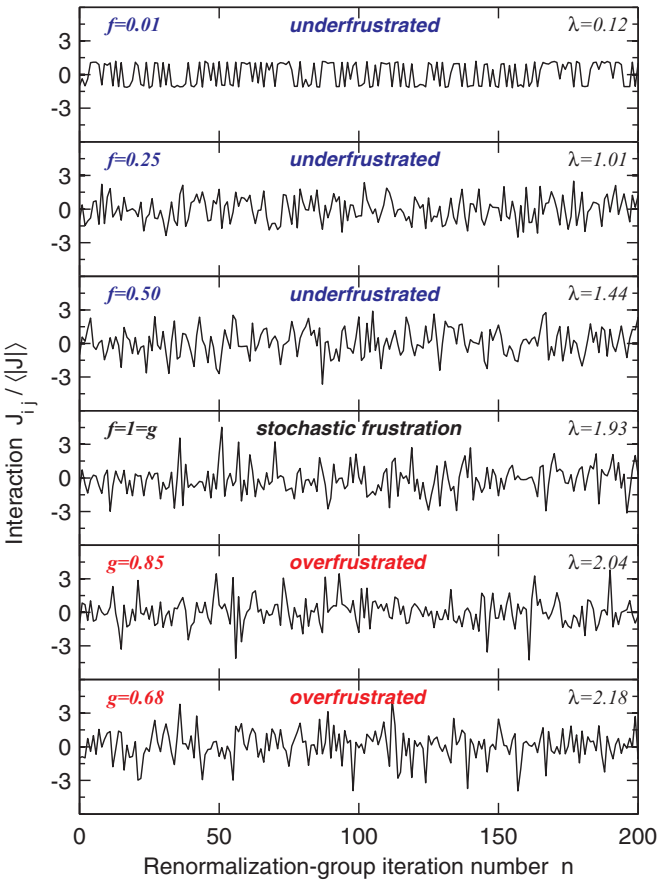

FIG. 6. (Color online) Interaction at a given position in the lattice at successive renormalization-group iterations, for $d = 3$ systems with different frustrations. In all cases, the antiferromagnetic bond concentration is $p = 0.5$ and the initial temperature is $1/J = 0.2$, inside the spin-glass phase. For each frustration amount, a chaotic trajectory of the interaction at a given position is seen. The calculated Lyapunov exponent for each case is given in the upper right corner of each panel.

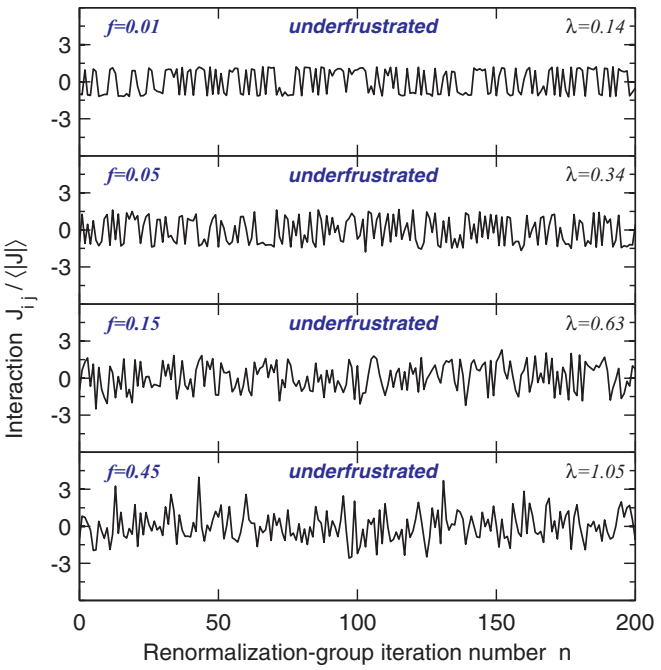

FIG. 7. (Color online) Interaction at a given position in the lattice at successive renormalization-group iterations, for $d = 2$ systems with different frustrations. In all cases, the antiferromagnetic bond concentration is $p = 0.5$ and the initial temperature is $1/J = 0.2$, inside the spin-glass phase. For each frustration amount, a chaotic trajectory of the interaction at a given position is seen. The calculated Lyapunov exponent for each case is given in the upper right corner of each panel.

interactions at a given position of the system are seen here as scaled with the average interaction $\langle|J|\rangle$ across the system, which diverges as b^{ny_R}, where n is the number of renormalization-group iterations and $y_R > 0$ is the **runaway exponent** shown in Fig. 10. This divergence indicates **strong-coupling chaotic behavior** [31]. In Figs. 6 and 7, it is seen that, for any amount of frustration, the local interaction at a given position in the lattice exhibits, under renormalization-group transformations, a chaotic trajectory [15].

The cumulative pictures of the chaotic visits of the consecutively renormalized interactions J_{ij} at a given position of the system, for a large number of renormalization-group iterations, in the spin-glass phases for different frustrations, is given for $d = 3$ and 2, respectively, in Figs. 8 and 9. It has been recently shown [31] that these distributions over renormalization-group iterations for a given position in the lattice are completely equivalent to the distributions of interactions across the lattice at a given renormalization-group iteration. As shown in Figs. 8 and 9, in the system where frustration is completely removed ($f = 0$, uppermost left-hand-side diagrams), the interaction at a given position randomly visits positive and negative values, giving the two δ functions shown in the figures. When frustration is introduced (f is increased from 0), these two δ functions broaden into two chaotic bands (shown in the figures for $f = 0.01$), which merge into a double-peaked single band (shown for $f = 0.10$), which transforms into a single peak (shown for $f = 0.25$). In $d = 3$, the single-peaked chaotic band continues through the stochastic frustration ($f = 1 = g$) into a range of overfrustrated systems ($g > 0.67$), albeit with varying Lyapunov exponents λ, as shown in the insets and in Fig. 10. In $d = 2$, the single-peaked chaotic band continues when frustration is increased to $f = 0.45$ (uppermost right-hand-side diagram), but no spin-glass phase occurs for $f > 0.49$, that is to say, in overfrustration, stochastic frustration, and the higher range of underfrustration.

The spin-glass phases, being chaotic, can be characterized [31] by the **Lyapunov exponent** of general chaotic behavior

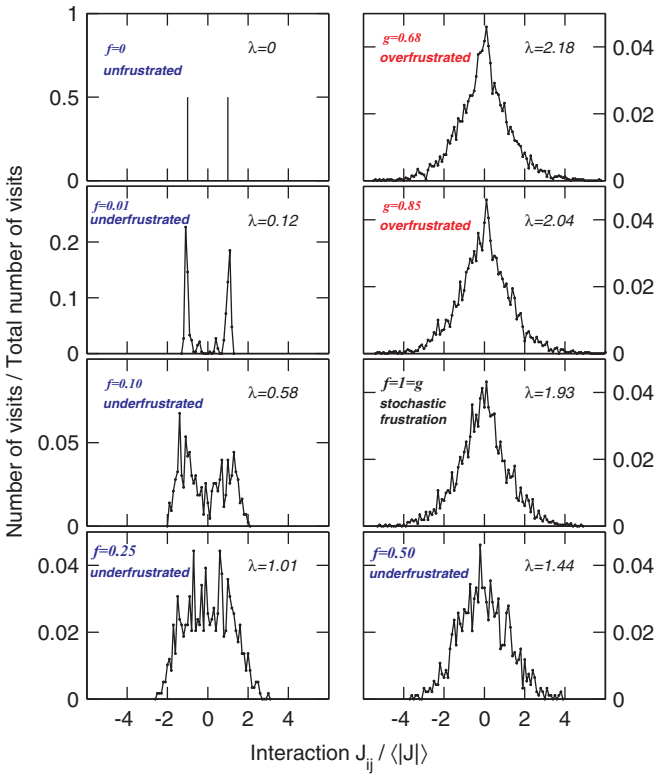

FIG. 8. (Color online) Chaotic visits of the consecutively renormalized interactions J_{ij} at a given position of the system, in the spin-glass phase of overfrustrated, underfrustrated, and stochastically frustrated Ising models in $d = 3$. These consecutively renormalized interactions at a given position of the system are shown here as scaled with the average interaction $\langle|J|\rangle$ across the system, which diverges as b^{ny_R}, where n is the number of renormalization-group iterations and $y_R > 0$ is the runaway exponent shown in Fig. 10. The number of visits into each interval of 0.1 on the horizontal axis has been scaled with the total number of renormalization-group iterations. Between 300 and 3500 renormalization-group iterations have been used for the different panels. The distributions of chaotic visits shown in the panels stabilize as the number of iterations is increased. The calculated Lyapunov exponent for each case is given in the upper right corner of each panel.

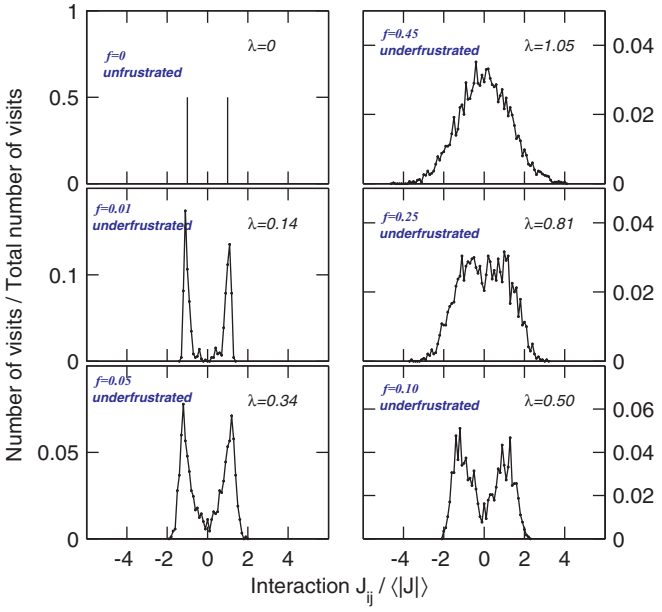

FIG. 9. (Color online) Chaotic visits of the consecutively renormalized interactions J_{ij} at a given position of the system, in the spin-glass phase of underfrustrated Ising models in $d = 2$. These consecutively renormalized interactions at a given position of the system are shown here as scaled with the average interaction $\langle|J|\rangle$ across the system, which diverges as b^{ny_R}, where n is the number of renormalization-group iterations and $y_R > 0$ is the runaway exponent shown in Fig. 10. The number of visits into each interval of 0.1 on the horizontal axis have been scaled with the total number of renormalization-group iterations. Between 700 and 5000 renormalization-group iterations have been used for the different panels. The distributions of chaotic visits shown in the panels stabilize as the number of iterations is increased. The calculated Lyapunov exponent for each case is given in the upper right corner of each panel. No spin-glass phase occurs for $f > 0.49$, as seen in Figs. 5 and 10.

[36,37]. The positivity of the Lyapunov exponent measures the strength of the chaos [36,37] and was also used in the previous spin-glass study of Ref. [27]. The calculation of the Lyapunov exponent is applied here to the chaotic renormalization-group trajectory at any specific position in the lattice,

$$\lambda = \lim_{n\to\infty} \frac{1}{n} \sum_{k=0}^{n-1} \ln \left| \frac{dx_{k+1}}{dx_k} \right|, \tag{7}$$

where $x_k = J_{ij}/\langle|J|\rangle$ are the interactions inside the smallest hierarchical unit at step k of the renormalization-group trajectory. The sum in Eq. (7) is to be taken within the asymptotic chaotic band. Thus, we throw out the first 100 renormalization-group iterations to eliminate the points outside of but leading to the chaotic band. Subsequently, typically using up to 2000 renormalization-group iterations in the sum in Eq. (7) ensures the convergence of the Lyapunov exponent value. The calculated Lyapunov exponents λ and runaway exponents y_R of the spin-glass phases of overfrustrated, underfrustrated, and stochastically frustrated Ising models in $d = 3$ (upper curves) and $d = 2$ (lower curves) are given in Fig. 10. As shown in this figure and in Figs. 6–9, as soon as frustration is introduced ($f > 0$), the Lyapunov exponent becomes positive and chaotic behavior occurs inside the spin-glass phase. Upon further increasing frustration, on the other hand, the spin-glass phase disappears when y_R reaches zero, as shown in Fig. 10, for $g = 0.67$ in $d = 3$ and $f = 0.49$ in $d = 2$.

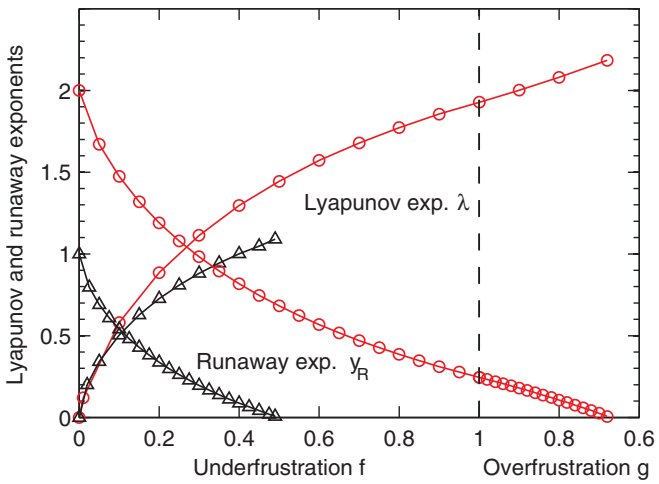

FIG. 10. (Color online) Lyapunov exponent λ and runaway exponent y_R of the spin-glass phases of overfrustrated, underfrustrated, and stochastically frustrated Ising models in $d = 3$ (upper curves) and $d = 2$ (lower curves). The horizontal scale shows, to the left of the dashed line, the f values of the underfrustrated cases and, to the right of the dashed line, the g values of the overfrustrated cases. The dashed line marks the stochastic frustration ($f = 1 = g$). As can be seen in this figure and in Figs. 8 and 9, as soon as frustration is introduced ($f > 0$), the Lyapunov exponent becomes positive and chaotic behavior occurs inside the spin-glass phase. The average interaction $\langle|J|\rangle$ across the system diverges as b^{ny_R}, where n is the number of renormalization-group iterations and $y_R > 0$ is the runaway exponent. The Lyapunov exponent λ monotonically increases with frustration from $\lambda = 0$ at zero frustration and the runaway exponent y_R monotonically decreases with frustration from $y_R = d - 1$ at zero frustration. The spin-glass phase disappears when y_R reaches zero, for $g = 0.67$ in $d = 3$ and $f = 0.49$ in $d = 2$.

V. ENTROPY AND SHORT- AND LONG-RANGE ORDER IN OVERFRUSTRATED AND UNDERFRUSTRATED SPIN GLASSES

Information about the relative shift and interchange in short- and long-range order can be deduced from entropy and specific-heat curves. Short-range order is deduced from a specific-heat peak (loss of entropy) that is away from the phase transition. Long-range order is deduced from the phase transition given by the renormalization-group flows. Thus, the characteristic temperature of short-range order is the temperature of the specific-heat peak. The characteristic temperature of long-range order is the phase transition temperature. The calculated entropy per site S/kN and specific heat per site C/kN are shown in Fig. 11 as a function of temperature $1/J$ at fixed antiferromagnetic bond concentration $p = 0.5$, for $d = 3$ systems with underfrustration ($f = 0.02,0.2,0.5$), stochastic frustration ($f = 1 = g$), and overfrustration ($g = 0.7$). The tick mark shows the phase transition point between the spin-glass phase and the paramagnetic phase for each frustration case. As also seen in Fig. 5, frustration lowers this transition temperature. For stochastic frustration ($f = 1 = g$), the specific-heat peak occurs outside the spin-glass phase, indicating that considerable short-range ordering occurs at higher temperatures before the onset of spin-glass long-range order. In contrast, for low frustration ($f = 0.02,0.2$), the specific-heat peak occurs inside the spin-glass phase, indicating that considerable short-range disorder persists into the higher temperatures of the spin-glass phase. This conclusion is also reached from the entropy curves in the upper panel. The changeover between these two regimes occurs for the underfrustrated system of $f = 0.5$. Overfrustrated systems show understandably specific-heat behavior similar to $f = 1$, with frustration lowering the long-range-order temperature and short-range order setting above this temperature with a specific-heat peak.

The calculated entropy per site S/kN as a function of the antiferromagnetic bond concentration p at fixed temperature $1/J = 0.5$ is shown in the upper panel of Fig. 12 for $d = 3$ systems with no frustration ($f = 0$), underfrustration ($f = 0.5,0.8$), stochastic frustration ($f = 1 = g$), and overfrustration ($g = 0.8$). Frustration is thus introduced at different rates in the different curves in Fig. 12. Here the tick mark shows the phase transition point between the ferromagnetic phase and the spin-glass phase for each frustration case. It is seen that frustration favors the spin-glass phase over the ferromagnetic phase. It is also seen that, as soon as frustration is introduced, the major portion of the entropy is created within the ferromagnetic phase as opposed to the spin-glass phase. Figure 12 also shows the calculated derivative of the entropy per site $(1/kN)(\partial S/k\partial p)$ as a function of the antiferromagnetic bond concentration p at fixed temperature $1/J = 0.5$, for the stochastic frustration system ($f = 1$) in $d = 3$. The tick mark again marks the phase transition point between the ferromagnetic phase and the spin-glass phase. The peak being inside the ferromagnetic phase also indicates that short-range disorder sets inside the ferromagnetic phase.

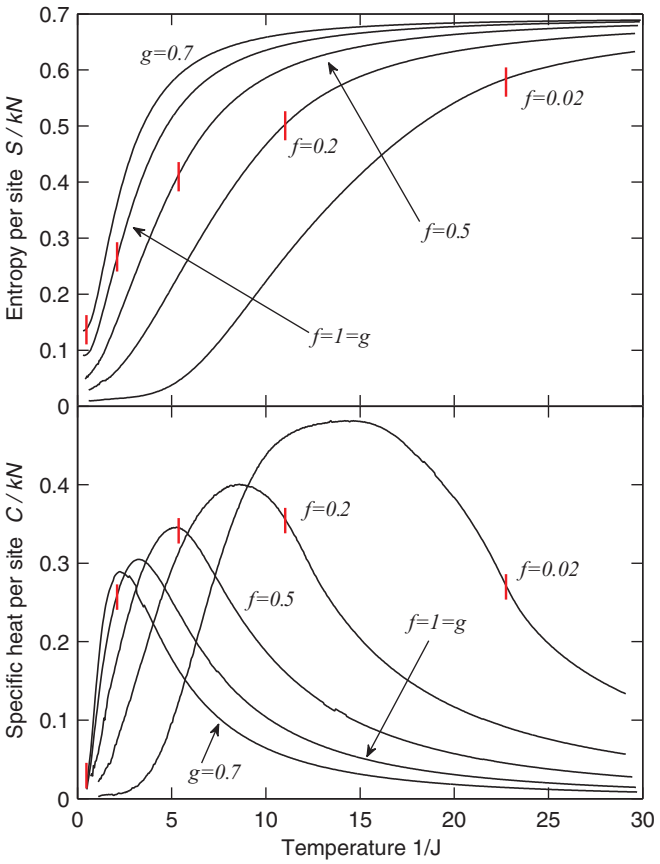

FIG. 11. (Color online) Calculated entropy per site S/kN (upper panel) and specific heat per site C/kN (lower panel) as a function of temperature $1/J$ at fixed antiferromagnetic bond concentration $p = 0.5$, for $d = 3$ systems with underfrustration ($f = 0.02, 0.2, 0.5$), the stochastic frustration ($f = 1 = g$), and overfrustration ($g = 0.7$). The tick mark shows the phase transition point between the spin-glass phase and the paramagnetic phase for each frustration case. It is seen that frustration lowers this transition temperature. Thus, for stochastic frustration ($f = 1 = g$), the specific-heat peak occurs outside the spin-glass phase, indicating that considerable short-range ordering occurs at higher temperatures before the onset of spin-glass long-range order. In contrast, for the more underfrustrated cases ($f = 0.02, 0.2$), the specific-heat peak occurs inside the spin-glass phase, indicating that considerable short-range disorder persists into the higher temperatures of the spin-glass phase. This conclusion is also reached from the entropy curves in the upper panel. The changeover between these two regimes occurs at the underfrustrated system of $f = 0.5$. Overfrustrated systems show understandably specific-heat behavior similar to $f = 1$, with frustration lowering the long-range-order temperature and short-range order setting at higher temperatures with a specific-heat peak.

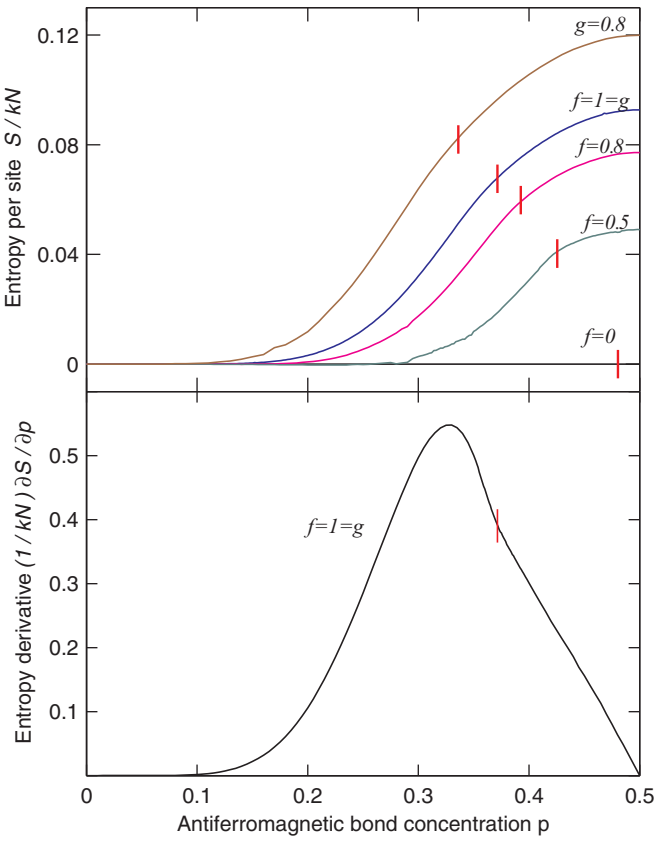

FIG. 12. (Color online) The top panel shows the calculated entropy per site S/kN as a function of the antiferromagnetic bond concentration p at fixed temperature $1/J = 0.5$, for systems with no frustration ($f = 0$), underfrustration ($f = 0.5, 0.8$), the stochastic frustration ($f = 1 = g$), and overfrustration ($g = 0.8$). The tick mark shows the phase transition point between the ferromagnetic phase and the spin-glass phase for each frustration case. It is seen that frustration favors the spin-glass phase over the ferromagnetic phase. It is also seen that, as soon as frustration is introduced, the major portion of the entropy is created within the ferromagnetic phase as opposed to the spin-glass phase. The lower panel shows the calculated derivative of the entropy per site $(1/kN)(\partial S/\partial p)$ as a function of the antiferromagnetic bond concentration p at temperature $1/J = 0.5$, for the stochastic frustration system ($f = 1$) in $d = 3$. The tick mark shows the phase transition point between the ferromagnetic phase and the spin-glass phase. The peak being inside the ferromagnetic phase shows that short-range disorder sets inside the ferromagnetic phase.

VI. CONCLUSION

This study started upon the realization that in Ising spin glasses, frustration can be adjusted continuously and, if needed, considerably, without changing the antiferromagnetic bond probability p, by using locally correlated quenched randomness, as we demonstrated here on hypercubic lattices and hierarchical lattices. Thus, a rich variety of spin-glass models and spin-glass phases was created. Such overfrustrated and underfrustrated systems on hierarchical lattices in $d = 3$ and 2 were studied in detail, yielding different information and insights. With the removal of just 51% of frustration ($f = 0.49$), a spin-glass phase appears in $d = 2$. With the addition of just 33% frustration ($g = 0.67$), the spin-glass phase disappears in $d = 3$. Sequences of phase diagrams for different levels of frustration have been calculated in both dimensions. In general, frustration lowers the spin-glass ordering temperature. At low temperatures, frustration favors the spin-glass phase (before it disappears) over the ferromagnetic phase and symmetrically the antiferromagnetic phase.

When any amount, including infinitesimal, frustration is introduced, the chaotic rescaling of local interactions occurs

in the spin-glass phase. Chaos increases with increasing frustration, as is seen from the increased positive value of the calculated Lyapunov exponent, starting from zero when frustration is absent. The calculated runaway exponent of the renormalization-group flows decreases, from $y_R = d - 1$ with increasing frustration to $y_R = 0$ when the spin-glass phase disappears.

From our calculations of entropy and specific-heat curves in $d = 3$, it is seen that frustration lowers in temperature the onset of both long- and short-range order in spin-glass phases, but is more effective on the former. Thus, for highly overfrustrated cases, considerable short-range order occurs in the lower-temperature range of the paramagnetic phase, whereas for moderately overfrustrated, stochastically frustrated, and underfrustrated cases, considerable short-range disorder occurs in the higher temperatures of the spin-glass phase. From calculations of the entropy and its derivative as a function of antiferromagnetic bond concentration p, it is seen that the ground-state and low-temperature entropy already mostly sets in within the ferromagnetic and antiferromagnetic phases, before the spin-glass phase is reached.

It is hoped that these calculational results, strictly valid for hierarchical lattices but suggestive for hypercubic lattices, would be repeated by Monte Carlo simulation, or other methods, for hypercubic lattices, as we have demonstrated the preparation of overfrustrated and underfrustrated hypercubic lattices.

ACKNOWLEDGMENTS

Support from the Alexander von Humboldt Foundation, the Scientific and Technological Research Council of Turkey, and the Academy of Sciences of Turkey is gratefully acknowledged.

[1] H. Nishimori, *Statistical Physics of Spin Glasses and Information Processing* (Oxford University Press, New York, 2001).
[2] A. N. Berker and L. P. Kadanoff, J. Phys. A **13**, L259 (1980).
[3] A. N. Berker and L. P. Kadanoff, J. Phys. A **13**, 3786 (1980).
[4] S. R. McKay, A. N. Berker, and S. Kirkpatrick, Phys. Rev. Lett. **48**, 767 (1982).
[5] S. R. McKay, A. N. Berker, and S. Kirkpatrick, J. Appl. Phys. **53**, 7974 (1982).
[6] G. Toulouse, Commun. Phys. **2**, 115 (1977).
[7] I. Morgenstern and K. Binder, Phys. Rev. Lett. **43**, 1615 (1979).
[8] D. C. Mattis, Phys. Lett. A **56**, 421 (1976).
[9] D. Blankschtein, M. Ma, and A. N. Berker, Phys. Rev. B **30**, 1362 (1984).
[10] L. W. Bernardi, K. Hukushima, and H. Takayama, J. Phys. A **32**, 1787 (1999).
[11] A. K. Murtazaev, I. K. Kamilov, and M. K. Ramazanov, Phys. Solid State **47**, 1163 (2005).
[12] H. T. Diep and H. Giacomini, *Frustated Spin Systems* (World Scientific, Singapore, 2005), pp. 1–58.
[13] V. Thanh Ngo, D. Tien Hoang, and H. T. Diep, J. Phys.: Condens. Matter **23**, 226002 (2011).
[14] A. N. Berker and S. R. McKay, J. Stat. Phys. **36**, 787 (1984).
[15] E. J. Hartford and S. R. McKay, J. Appl. Phys. **70**, 6068 (1991).
[16] F. Krzakala, Europhys. Lett. **66**, 847 (2004).
[17] F. Krzakala and J. P. Bouchaud, Europhys. Lett. **72**, 472 (2005).
[18] M. Sasaki, K. Hukushima, H. Yoshino, and H. Takayama, Phys. Rev. Lett. **95**, 267203 (2005).
[19] J. Lukic, E. Marinari, O. C. Martin, and S. Sabatini, J. Stat. Mech. (2006) L10001.
[20] P. Le Doussal, Phys. Rev. Lett. **96**, 235702 (2006).
[21] T. Rizzo and H. Yoshino, Phys. Rev. B **73**, 064416 (2006).
[22] H. G. Katzgraber and F. Krzakala, Phys. Rev. Lett. **98**, 017201 (2007).
[23] H. Yoshino and T. Rizzo, Phys. Rev. B **77**, 104429 (2008).
[24] T. Aspelmeier, Phys. Rev. Lett. **100**, 117205 (2008).
[25] T. Aspelmeier, J. Phys. A **41**, 205005 (2008).
[26] T. Mora and L. Zdeborova, J. Stat. Phys. **131**, 1121 (2008).
[27] N. Aral and A. N. Berker, Phys. Rev. B **79**, 014434 (2009).
[28] T. E. Stone and S. R. McKay, Physics A **389**, 2911 (2010).
[29] T. Jörg and F. Krzakala, J. Stat. Mech. (2012) L01001.
[30] T. Obuchi and K. Takahashi, J. Phys. A **45**, 125003 (2012).
[31] E. Ilker and A. N. Berker, Phys. Rev. E **87**, 032124 (2013).
[32] F. Roma and S. Risau-Gusman, Phys. Rev. E **88**, 042105 (2013).
[33] W.-K. Chen, Ann. Probab. **41**, 3345 (2013).
[34] L. A. Fernandez, V. Martin-Mayor, G. Parisi, and B. Seoane, Europhys. Lett. **103**, 67003 (2013).
[35] W. de Lima, G. Camelo-Neto, and S. Coutinho, Phys. Lett. A **377**, 2851 (2013).
[36] P. Collet and J.-P. Eckmann, *Iterated Maps on the Interval as Dynamical Systems* (Birkhäuser, Boston, 1980).
[37] R. C. Hilborn, *Chaos and Nonlinear Dynamics*, 2nd ed. (Oxford University Press, New York, 2003).
[38] A. A. Migdal, Zh. Eksp. Teor. Fiz. **69**, 1457 (1975) [Sov. Phys. JETP **42**, 743 (1976)].
[39] L. P. Kadanoff, Ann. Phys. (NY) **100**, 359 (1976).
[40] A. N. Berker and S. Ostlund, J. Phys. C **12**, 4961 (1979).
[41] R. B. Griffiths and M. Kaufman, Phys. Rev. B **26**, 5022R (1982).
[42] M. Kaufman and R. B. Griffiths, Phys. Rev. B **30**, 244 (1984).
[43] S. R. McKay and A. N. Berker, Phys. Rev. B **29**, 1315 (1984).
[44] M. Hinczewski and A. N. Berker, Phys. Rev. E **73**, 066126 (2006).
[45] D. Andelman and A. N. Berker, Phys. Rev. B **29**, 2630 (1984).
[46] G. Migliorini and A. N. Berker, Phys. Rev. B **57**, 426 (1998).
[47] M. Hinczewski and A. N. Berker, Phys. Rev. B **72**, 144402 (2005).
[48] C. Güven, A. N. Berker, M. Hinczewski, and H. Nishimori, Phys. Rev. E **77**, 061110 (2008).
[49] G. Gülpınar and A. N. Berker, Phys. Rev. E **79**, 021110 (2009).
[50] M. J. P. Gingras and E. S. Sørensen, Phys. Rev. B **46**, 3441 (1992).
[51] M. J. P. Gingras and E. S. Sørensen, Phys. Rev. B **57**, 10264 (1998).
[52] S.-C. Chang and R. Shrock, Phys. Lett. A **377**, 671 (2013).
[53] R. F. S. Andrade and H. J. Herrmann, Phys. Rev. E **87**, 042113 (2013).
[54] R. F. S. Andrade and H. J. Herrmann, Phys. Rev. E **88**, 042122 (2013).
[55] C. Monthus and T. Garel, J. Stat. Mech. (2013) P06007.

[56] O. Melchert and A. K. Hartmann, Eur. Phys. J. B **86**, 323 (2013).
[57] J.-Y. Fortin, J. Phys.: Condens. Matter **25**, 296004 (2013).
[58] Y. H. Wu, X. Li, Z. Z. Zhang, and Z. H. Rong, Chaos Solitons Fractals **56**, 91 (2013).
[59] M. E. Fisher and A. N. Berker, Phys. Rev. B **26**, 2507 (1982).
[60] S. B. Roy and M. K. Chattopadhyay, Phys. Rev. B **79**, 052407 (2009).
[61] J. O. Indekeu and A. N. Berker, Physica A **140**, 368 (1986).
[62] R. R. Netz and A. N. Berker, Phys. Rev. Lett. **68**, 333 (1992).
[63] M. G. Mazza and M. Schoen, Int. J. Mol. Sci. **12**, 5352 (2011).
[64] S. Chen, H.-B. Luo, H.-L. Xie, and H. L. Zhang, J. Polym. Sci. A **51**, 924 (2013).
[65] H. Nishimori, Prog. Theor. Phys. **66**, 1169 (1981).
[66] H. Nishimori and K. Nemoto, J. Phys. Soc. Jpn. **71**, 1198 (2002).
[67] J.-M. Maillard, K. Nemoto, and H. Nishimori, J. Phys. A **36**, 9799 (2003).
[68] K. Takeda and H. Nishimori, Nucl. Phys. B **686**, 377 (2004).
[69] K. Takeda, T. Sasamoto, and H. Nishimori, J. Phys. A **38**, 3751 (2005).